



0092-8240(95)00359-2

CODING OF STIMULUS INTENSITY IN AN OLFACTORY RECEPTOR NEURON: ROLE OF NEURON SPATIAL EXTENT AND PASSIVE DENDRITIC BACKPROPAGATION OF ACTION POTENTIALS

■ A. VERMEULEN,^{*†} J.-P. ROSPARS,^{**} P. LÁNSKÝ[§], and
H. C. TUCKWELL^{||*}

^{*}Laboratoire de Biométrie,
Institut National de la Recherche Agronomique,
Route de Saint-Cyr,
78026 Versailles Cedex, France

[†]Laboratoire de Traitement d'Images et Reconnaissance de Formes,
Institut National Polytechnique,
46 avenue Félix Viallet,
38031 Grenoble Cedex, France

[§]Institute of Physiology,
Academy of Sciences of the Czech Republic,
Videňská 1083,
142 20 Prague 4,
Czech Republic

^{||}School of Mathematical Sciences,
Centre for Mathematics and Its Applications,
Australian National University,
Canberra, ACT 0200, Australia

The olfactory receptor neuron provides a good opportunity to analyze a biophysical model of a single neuron because its dendritic structure is simple and even close to a cylinder in the case of the moth sex-pheromone receptor cell. We have considered this cylindrical case and studied two main problems. First, we were concerned with the effect of the neuron's length on the receptor potential for a constant stimulus-induced conductance change. An analytical solution for the receptor potential was determined by using input resistances. It was shown that the longer the neuron, the greater its ability to code over a wide range of values of the intensity of the stimulus. Second, we studied numerically the passive backpropagation of action potentials into the dendrite and its influence on the firing frequency. While propagating along the dendrite the action potential decreases in amplitude and its shape becomes rounded. The firing frequency in the model with backpropagation was found to be greater than that obtained analytically in the absence of backpropagation. However, for any given conductance change, when normalized with respect to their maxima, both firing frequencies

[†]Author to whom correspondence should be addressed.

were found to be very similar over a wide range of parameter values. Therefore, the actual firing rate (with backpropagation) may be approximated by the analytical solution without backpropagation if the actual firing rate for a large conductance change is known.

1. Introduction. As pointed out recently by Abbott (1992, 1994), the determination of the potential distributions throughout neuronal structures is a classical problem in theoretical neurobiology; see, for example, Segev (1992) for a succinct account. It was demonstrated many years ago by Hodgkin and Rushton (1946) that subthreshold responses of nerve cylinders could be predicted accurately by the use of linear cable theory. It was a natural development, therefore, that when attention was focussed on neurons with complex anatomies, the first approach adopted consisted of attempts to extend cable theory to such cells.

The origins of most present-day research in this area can be traced to the pioneering work of Rall (1960, 1962, 1964) which he has summarized along with more recent developments; see Rall (1977, 1989). The early work in this domain focussed on the neurophysiological properties of motoneurons, but there has also been much interest in other types of nerve cells (Claiborne *et al.*, 1992; Wilson, 1992; Segev *et al.*, 1992). In most applications of cable theory the three-halves-power law for diameters at branch points has been assumed to enable the complex geometry of dendritic trees to be avoided by mapping the potential onto that of an equivalent cylinder (Rall, 1964), or by a somewhat more general procedure (Walsh and Tuckwell, 1985; Tuckwell, 1988a). In most cases, therefore, an analytical approach can be used to compute the distribution of potential and this, with the invention of certain procedures (Butz and Cowan, 1974; Abbott, 1992), also has been possible when other geometries have been considered.

Modeling an olfactory receptor neuron provides an excellent opportunity to apply cable theory to develop a biophysical model of a neuron because its dendritic structure is simple. In the case of the moth sex-pheromone receptor cell it can even be accurately approximated by that of a cylinder (Keil, 1984). Odorant coding begins by *transduction* which occurs in the odorant-sensitive part of the dendrite. The binding of odorant molecules to receptor proteins borne by the membrane triggers a second-messenger system which finally opens odorant-dependent ionic channels (see Stengl *et al.*, 1992) whereupon a membrane depolarization, called the *receptor potential*, is evoked. When this potential is high enough, *action potentials* are generated and propagated along the antennal or olfactory nerve to the brain (Kaissling, 1986). We proposed (Lánský *et al.*, 1994; Rospars *et al.*, 1995) a model describing this sequence of events. This model is composed of three functional modules: the *transduction*, *receptor potential* and *action potential* modules. The membrane of the receptor neuron is modeled by a

cylindrical cable which is divided in two parts (Fig. 1a); (i) an odorant-sensitive dendrite containing the transduction mechanisms and (ii) an odorant-insensitive part corresponding to passive dendrite, soma, initial segment and axon.

In the present work, part of which has appeared in preliminary form elsewhere (Vermeulen *et al.*, 1995), we focus our attention on the receptor and action potential modules. The odorant concentration is assumed to be constant. Consequently, the transduction module is in a steady state and the number of open odorant-dependent ionic channels is constant. These open channels are modeled by a constant odorant-dependent conductance which is considered here as the input signal of the receptor potential

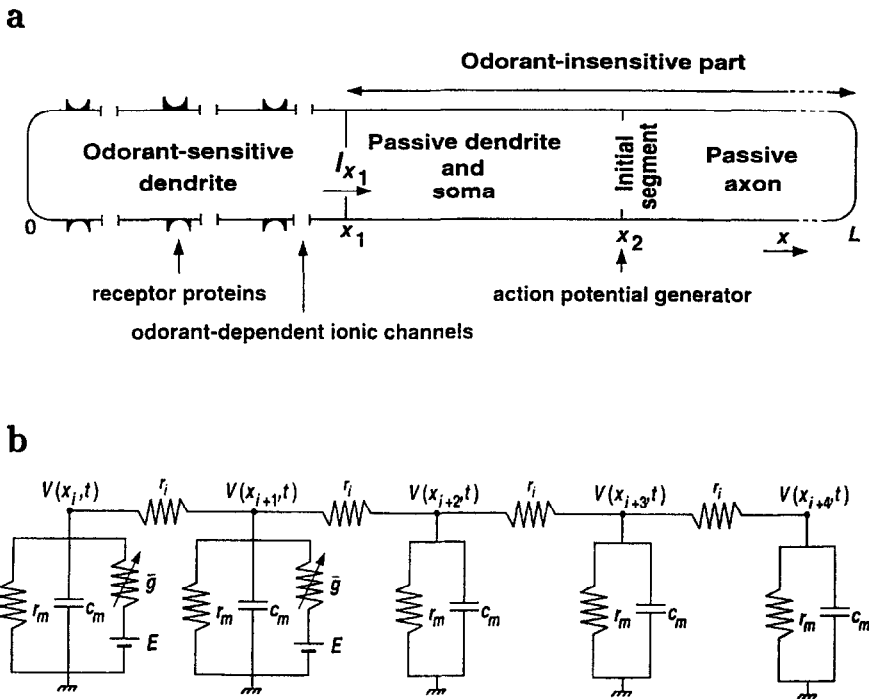


Figure 1. Schematic representation of the olfactory receptor neuron (a) and equivalent circuit corresponding to the odorant-sensitive dendrite and passive parts (b). The neuron is modeled by a cylindrical cable which is divided into an odorant-sensitive dendrite with transduction mechanisms and an odorant-insensitive part, corresponding to passive dendrite, soma, initial segment and axon. Assuming a constant odorant concentration, the receptor potential $V(x, t)$ is evoked by an odorant-dependent conductance which is uniform and constant (\bar{g}) on the odorant-sensitive dendrite and zero elsewhere. When the potential at the initial segment $V(x_2, t)$ is high enough, action potentials are generated (see Fig. 5). In (b), a uniform discretization in space is used and the neuron's terminals are "sealed." Parameters: $\Delta x = 1$, $x_1 = 2$, $L = 5$.

module. Two main problems will be addressed:

1. Experimental observations show that the range of variation of the receptor potential in certain receptor neurons, for example, the sex-pheromone receptors of moths (see Kaissling, 1987) extends over more than six decades of odorant concentration. In previous work (Rospars *et al.*, 1995) we studied this range in a semi-infinite model neuron. Here, we show that in a point model neuron the coding range extends over only about 2.5 decades of the odorant-dependent conductance change and we study how it depends on the length of the neuron.
2. In Lánský *et al.* (1994) and Rospars *et al.* (1995) we determined analytically the dependency of the firing frequency on the odorant-dependent conductance without considering the passive backpropagation effect of action potentials in the dendrite after their generation at the axon initial segment. The need arises to estimate the magnitude of the backpropagation effect on the firing rate. In order to address this we will determine numerically the frequency–conductance relation for a model which takes into account backpropagation and compare it to the relation found analytically.

2. Methods. The membrane potential $V(x, t)$ that results from a given conductance change $g(x, t)$ is given by the cable equation (see, for example, Tuckwell 1988b, Chap. 7),

$$\frac{\partial V(x, t)}{\partial t} = \frac{\partial^2 V(x, t)}{\partial x^2} - V(x, t) + g(x, t)(E - V(x, t)), \quad 0 < x < L, \quad (1)$$

where L is the total length of the neuron, x is the distance along the neuron expressed in units of the characteristic length or space constant λ ($= \sqrt{r_m/r_i}$, with r_m the resistance of unit length times unit length and r_i is the axial resistance of the internal medium per unit length) and t is the time expressed in units of the time constant τ ($= c_m r_m$, with c_m the membrane capacitance per unit length). Furthermore, E is the reversal potential of the ions that cross the membrane when the odorant receptor sites are activated and $g(x, t)$ is the increase in membrane conductance due to these ions expressed in units of the resting membrane conductance (r_m^{-1}). The external medium is assumed to be uniform and the resting potential is set to zero. An electrical circuit equivalent to (1) with a uniform discretization in space and a constant conductance change over the odorant-sensitive dendrite is shown in Fig. 1b.

The space-time solutions of this partial differential equation were determined numerically. Equation (1) was approximated by a system of coupled difference equations, obtained by replacing the space derivatives with finite differences,

$$\frac{dV(t)}{dt} = \frac{V_{i+1}(t) - 2V_i(t) + V_{i-1}(t)}{(\Delta x)^2} - V_i(t) + g_i(t)(E - V_i(t)), \quad (2)$$

where $V_i(t) = V(x_i, t)$, $g_i(t) = g(x_i, t)$ and $x_i = i \Delta x$ in the case of a uniform discretization with $i = 0, 1, 2, \dots$. This system was then integrated using an implicit (or backward) Euler method to obtain a system of coupled difference equations (Mascagni, 1989),

$$\frac{V_i^{j+1} - V_i^j}{\Delta t} = \frac{V_{i+1}^{j+1} - 2V_i^{j+1} + V_{i-1}^{j+1}}{(\Delta x)^2} - V_i^{j+1} + g_i^{j+1}(E - V_i^{j+1}), \quad (3)$$

where $V_i^j = V(x_i, t_j)$, $g_i^j = g(x_i, t_j)$ and $t_j = j \Delta t$ with $j = 0, 1, 2, \dots$.

The approximation used a uniform mesh in space (step size $\Delta x = 0.2$ space constant). Three points were added to the mesh, one on both sides of the proximal end x_1 of the odorant-sensitive dendrite (Fig. 1a) to improve the precision of the numerical solution, and one at the axon initial segment x_2 to guarantee its inclusion. When the numerical solution for a large time t (so approximating the steady state) without closing the switch was compared with the analytical solution (13), it was found that the maximum error on V was always at x_1 and that the addition of two points very close to the discontinuity x_1 ($x_1 \pm 0.001$) could greatly reduce this error.

The implicit Euler method was used to avoid numerical instabilities or oscillations during the rising and falling phases of the action potential, i.e. when the membrane potential changes rapidly (Mascagni, 1989). This method was used in combination with an adaptive time step. This step was kept at a minimum value (0.001 time constant) during the rise and fall of the action potential. Then, after the action potential, it was increased at every time step by 15% until it reached a maximum value (0.05). These step sizes were chosen to be small to improve the precision, the implicit Euler method being only of first order (Mascagni, 1989). We found that the spiking frequencies were not appreciably changed when the step sizes were increased by a factor of 10.

3. Receptor Potential

Analytical steady-state solution for a uniformly stimulated odorant-sensitive dendrite. Consider first the steady-state solution of (1) when the conductance is a positive constant \bar{g} over the odorant-sensitive dendrite and zero

elsewhere,

$$g(x, t) = \bar{g}(1 - H(x - x_1)), \quad 0 \leq x \leq L, \quad (4)$$

where $H(x)$ is the unit (Heaviside) step function and x_1 ($0 < x_1 < L$) corresponds to the border between the odorant-sensitive dendrite and the odorant-insensitive part (Fig. 1a). From (1) and (4), the steady-state potential, which we also designate by V , must satisfy the ordinary differential equation

$$-\frac{d^2V(x)}{dx^2} + V(x) = \bar{g}(1 - H(x - x_1))(E - V(x)), \quad 0 < x < L. \quad (5)$$

Its solutions may be determined first for the odorant-sensitive dendrite (from 0 to x_1), then for the odorant-insensitive part, which includes the passive dendrite and the whole axon (from x_1 to L). This approach is appropriate because both parts are defined separately and the solution for the first part uses only the input resistance of the odorant-insensitive part.

Let us consider first the odorant-sensitive dendrite. The general solution of (5) is given by

$$V(x) = c_1 \exp(-\sqrt{1 + \bar{g}}x) + c_2 \exp(\sqrt{1 + \bar{g}}x) + \frac{\bar{g}E}{\bar{g} + 1}, \quad 0 \leq x \leq x_1, \quad (6)$$

where c_1 and c_2 are constants to be determined by using the boundary conditions at the beginning ($x = 0$) and end ($x = x_1$) of the odorant-sensitive dendrite. By considering that no current flows at $x = 0$, which is the so-called sealed end condition (see Tuckwell 1988a), the first boundary condition is

$$V'(0) = 0, \quad (7)$$

where the prime indicates differentiation with respect to x . This condition applied to (6) gives $c_1 = c_2$ and thus

$$V(x) = 2c_1 \cosh(\sqrt{1 + \bar{g}}x) + \frac{\bar{g}E}{\bar{g} + 1}, \quad 0 \leq x \leq x_1. \quad (8)$$

We utilize the definition of the steady-state axial current $I_i(x_1)$ at $x = x_1$,

$$I_i(x_1) = -\frac{V'(x_1)}{r_i}, \quad (9)$$

in conjunction with the input resistance $R_{in} = V(x_1)/I_i(x_1)$ of the odorant-insensitive part, to obtain the second boundary condition:

$$V(x_1) = -\frac{R_{in}}{r_i}V'(x_1). \tag{10}$$

From (8) and (10) one finds

$$c_1 = -\frac{1}{2} \frac{1}{\alpha\sqrt{1+\bar{g}} \sinh(\sqrt{1+\bar{g}}x_1) + \cosh(\sqrt{1+\bar{g}}x_1)} \frac{\bar{g}E}{\bar{g}+1} \tag{11}$$

with $\alpha = R_{in}/r_i$. Replacing c_1 in (8) by its expression (11) gives for the odorant-sensitive dendrite

$$V(x) = \left(1 - \frac{\cosh(\sqrt{1+\bar{g}}x)}{\alpha\sqrt{1+\bar{g}} \sinh(\sqrt{1+\bar{g}}x_1) + \cosh(\sqrt{1+\bar{g}}x_1)} \right) \frac{\bar{g}E}{\bar{g}+1}, \tag{12}$$

$0 \leq x \leq x_1.$

Consider now the odorant-insensitive part. The receptor potential at its proximal boundary is given by (12) with $x = x_1$, by continuity. This boundary condition is equivalent to the injection of a steady-state current (see (9)), which is a classical case described, for example, by Rall (1989) and Tuckwell (1988a, Table 4.2), who give the potential $V(x)$ and input resistance for a semi-infinite cable and finite cables with either a sealed end or a killed end, as follows.

In the case where the odorant-insensitive part is a finite cable of length $L - x_1$ with a sealed axon terminal, the input resistance is $R_{in} = r_i \coth(L - x_1)$ and the receptor potential on this cable part is $V(x_1)\cosh(L - x)/\cosh(L - x_1)$. Then the complete solution is

$$V(x) = \begin{cases} \left(1 - \frac{\cosh(\sqrt{1+\bar{g}}x)}{\sqrt{1+\bar{g}} \coth(L-x_1)\sinh(\sqrt{1+\bar{g}}x_1) + \cosh(\sqrt{1+\bar{g}}x_1)} \right) \frac{\bar{g}E}{\bar{g}+1}, & 0 \leq x \leq x_1, \\ V(x_1) \frac{\cosh(L-x)}{\cosh(L-x_1)}, & x_1 < x \leq L. \end{cases} \tag{13}$$

Some examples of the receptor potential (13) for different conductance changes and different lengths of the neuron and the odorant-sensitive dendrite are shown in Fig. 2. In the case $L = x_1$ one finds from (13) that the potential $V = \bar{g}E/(\bar{g} + 1)$ is independent of x . This is the same potential as that found in a point model neuron ($L = 0$).

Another case of interest, useful to describe the membrane potential when an action potential generator is added (see section 3.2), consists in keeping the receptor potential at zero at a given point x_2 (corresponding to the axon initial segment) which is the "killed end" or "short-circuit" boundary condition. In this case the input resistance (Table 4.2 in Tuckwell, 1988a) is $R_{in} = r_i \tanh(L - x_1)$ and the receptor potential (from same table and (11)) is

$$V(x) = \begin{cases} \left(1 - \frac{\cosh(\sqrt{1 + \bar{g}} x)}{\sqrt{1 + \bar{g}} \tanh(x_2 - x_1) \sinh(\sqrt{1 + \bar{g}} x_1) + \cosh(\sqrt{1 + \bar{g}} x_1)} \right) \frac{\bar{g}E}{\bar{g} + 1}, & 0 \leq x \leq x_1, \\ V(x_1) \frac{\sinh(x_2 - x)}{\sinh(x_2 - x_1)}, & x_1 < x \leq x_2. \end{cases} \quad (14)$$

An example of this potential as a function of x is shown in Fig. 3.

Dependence of receptor potential on odorant-dependent conductance and neuron length. We now wish to study the dependence of the receptor potential at the axon initial segment x_2 on the conductance \bar{g} for different lengths L . Equation (13) shows that the location of the initial segment influences the magnitude of the receptor potential. Since we are not directly interested in the influence of this location, we introduce the relative receptor potential $V^*(x)$, which is the ratio of the receptor potential $V(x)$ at any point for a given conductance \bar{g} to the maximum possible value of the receptor potential $V_M(x)$ at the same point when $\bar{g} \rightarrow \infty$:

$$V^*(x) = \frac{V(x)}{V_M(x)}. \quad (15)$$

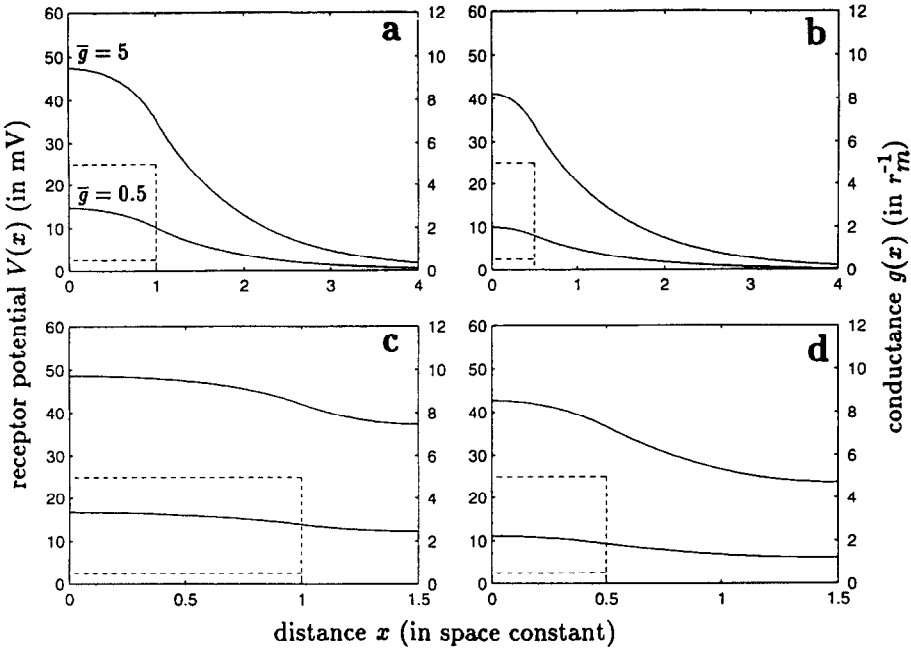


Figure 2. Receptor potential $V(x)$ along the neuron (solid line) for a conductance change $g(x)$ (dashed line) with $\bar{g} = 0.5$ and $\bar{g} = 5$, different lengths of the neuron and different lengths of the odorant-sensitive dendrite. (a) $L = 7$ and $x_1 = 1$; (b) $L = 7$ and $x_1 = 0.5$; (c) $L = 1.5$ and $x_1 = 1$; (d) $L = 1.5$ and $x_1 = 0.5$. Parameter: $E = 60$.

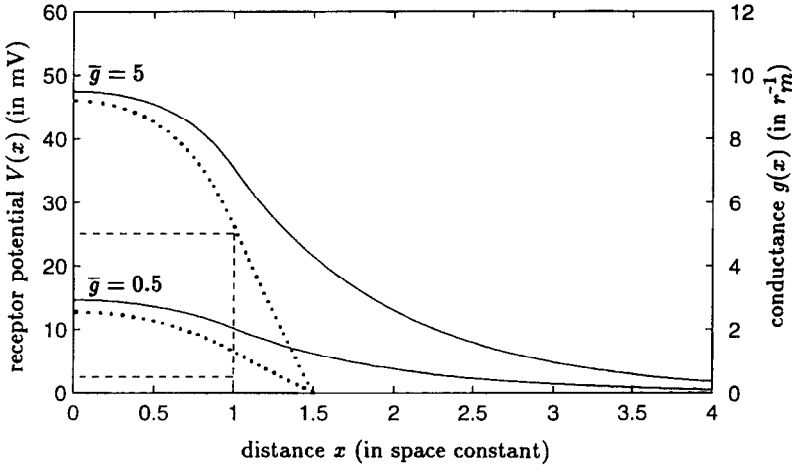


Figure 3. Receptor potential $V(x)$ along a semi-infinite neuron for a conductance change $g(x)$ (dashed line) with $\bar{g} = 0.5$ and $\bar{g} = 5$, without (solid line) and with (dotted line) dendritic backpropagation of action potentials. In the latter case, we consider a refractory period $T_r \rightarrow \infty$. Parameters: $x_1 = 1$, $x_2 = 1.5$, $E = 60$ and $E_{\text{down}} = 0$.

Using equation (13), the relative receptor potential on the odorant-insensitive part simplifies to

$$V^*(x) = \frac{V(x_1)}{V_M(x_1)} = \frac{V(x_1)}{E}, \quad x_1 \leq x \leq L. \quad (16)$$

Equation (16) shows that $V^*(x)$ is a constant V^* on the odorant-insensitive part ($x_1 \leq x \leq L$). In this form the expression of the receptor potential becomes independent of the position of the initial segment.

The relative receptor potential V^* as a function of $\log \bar{g}$ is shown in Fig. 4a, based on (13), i.e. in the case of a neuron with a sealed end at the axon terminal, for different neuron lengths L and the realistic value $x_1 = 1$. For comparison the same relation is shown for a point model neuron which, as seen before, is equivalent to a neuron with uniform stimulation and no odorant-insensitive part, i.e. $L = x_1$ in (13). Whatever L , V^* is a sigmoid function of $\log \bar{g}$. This curve presents two significant features from the point of view of intensity coding: its position along the conductance axis and the range of conductances that it can code.

The first feature can be characterized by the conductance at half maximal response, i.e. the conductance for $V^* = 0.5$. This conductance depends on L and increases from $\bar{g} = 1$ for $L = 0$ to $\bar{g} \approx 3$ for $L \rightarrow \infty$ (Fig. 4a and b).

The coding range for conductance is related to the slope of the curve. It may be defined as the values of \bar{g} over which the receptor potential V^* increases from an arbitrary small value ϵ (threshold conductance) to $1 - \epsilon$ (saturating conductance), for example from 0.05 to 0.95 (see solid arrows in Fig. 4a for a long cable). If the conductance changes over a wide range of values, it is more appropriate to define the coding range Δ_g as the difference between the logarithms of the threshold conductance and the saturating conductance. This difference corresponds to the length (in decades) of the arrow shown in Fig. 4b. As shown in Fig. 4c the conductance range increases with the neuron length L from a minimum of about 2.5 decades for a point model neuron to an asymptotic maximum of about 3.5 decades for a long neuron ($L = 4$ or more). Therefore, the greater the spatial extent of the receptor neuron, the greater its ability to code over a wide range of values of the intensity of the stimulus. Because the conductance at $V^* = 0.05$ changes only slightly with L (from about 0.05 to about 0.12), the increase of Δ_g with L is due mainly to the shift toward higher conductances of the upper bound ($V^* = 0.95$) from about 20 to about 400, as shown in Fig. 4a and b.

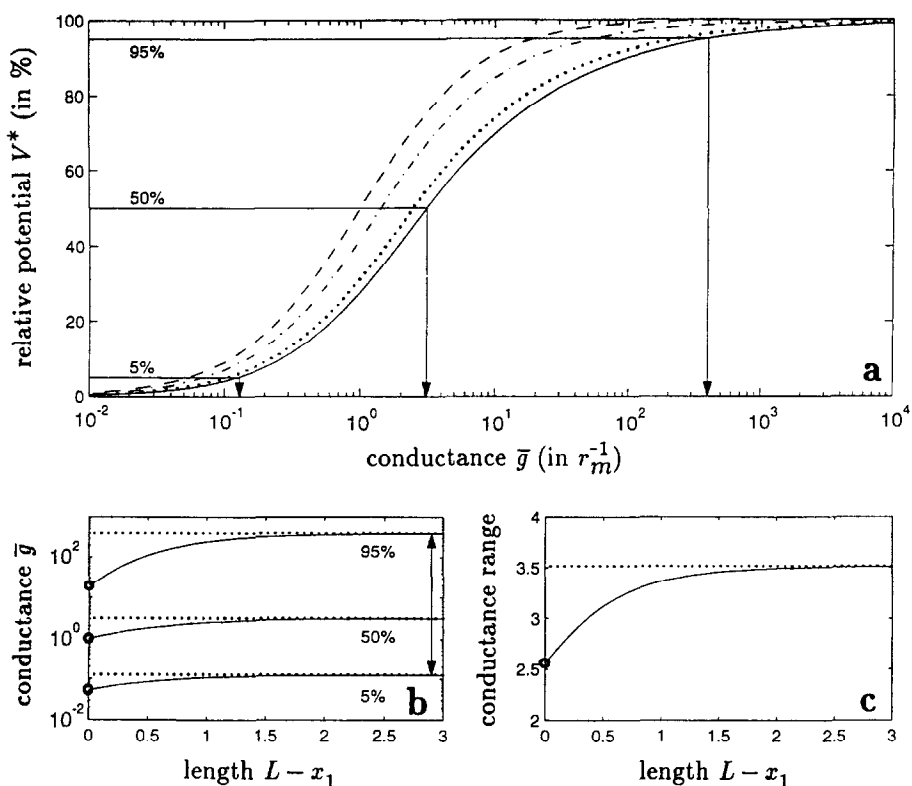


Figure 4. Receptor potential for the cylinder cable neuron of Fig. 1b. (a) Relative receptor potential V^* at the axon initial segment in percent of its maximum value (E) as a function of the odorant-dependent conductance \bar{g} for different lengths of the odorant-insensitive part, $L - x_1 = 0$ (dash, equivalent to a point model neuron), 0.25 (dash-dot), 1 (dot) and 4 (solid). In all cases the axon terminal at L is sealed. The arrows give the conductances \bar{g} for $V^* = 5, 50$ and 95% in a long cable. (b) Conductance \bar{g} (in r_m^{-1}) for $V^* = 5, 50$ and 95% as a function of L (in space constants). The length of the arrow (\leftrightarrow , in decades) corresponds to the conductance range for a long cable. (c) Conductance range (in decades) for the 5–95% interval of V^* as a function of L (in space constant). In (b) and (c), the circles correspond to a point model neuron and the dotted lines to the asymptotic values when $L \rightarrow \infty$. Parameter: $x_1 = 1$.

4. Action potentials

Generation of action potentials. The axon initial segment is represented by the circuit shown in Fig. 5a and b with four branches in parallel consisting of a capacitance, a resistance and two batteries E_{up} and E_{down} with a common switch. The switch can close either the branch with the battery E_{up} (corresponding to the equilibrium potential of sodium ions) or the branch with the battery E_{down} (equilibrium potential of the potassium ions). This circuit generates a square pulse as follows. When the potential

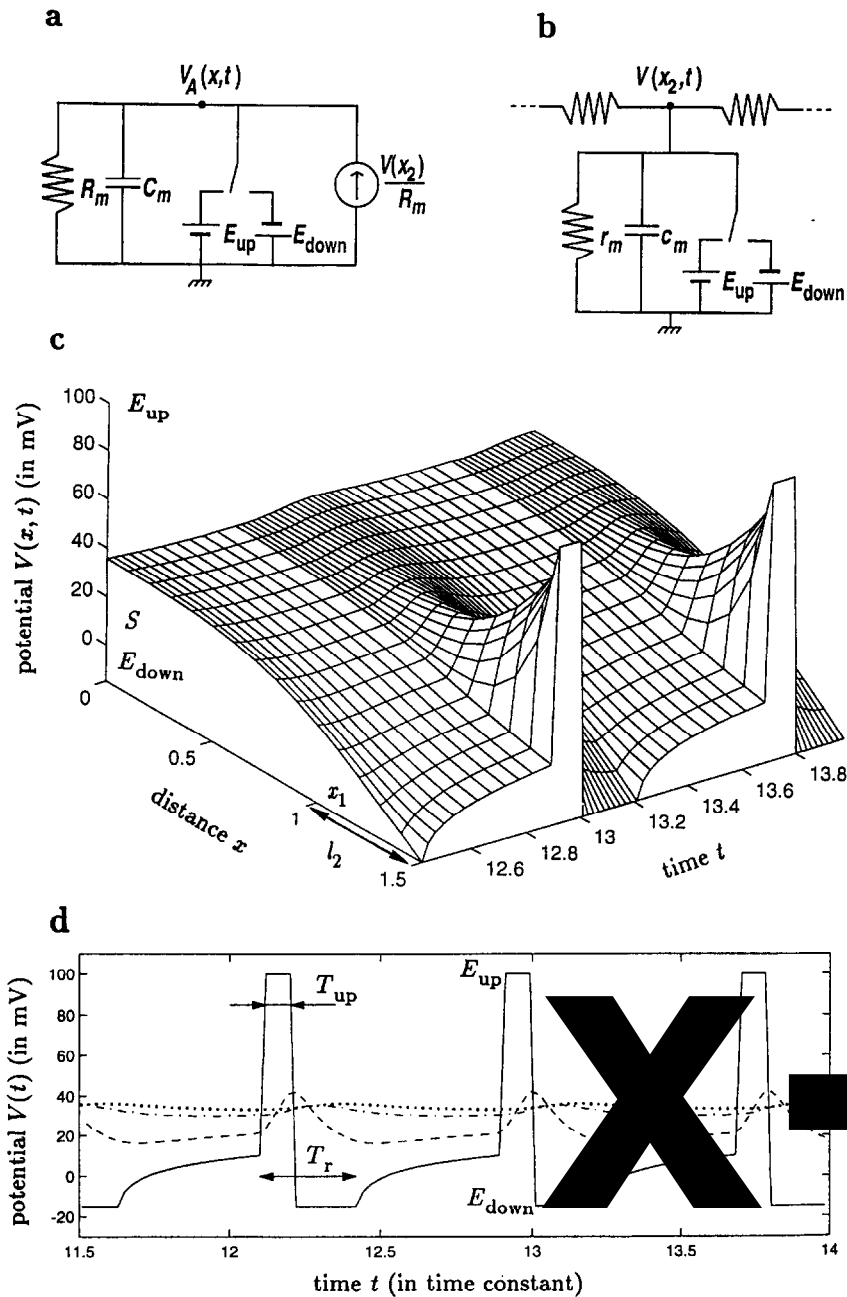


Figure 5. Equivalent circuits of the action potential generator with (a) and without (b) backpropagation of the action potentials into the dendrite. (c) Profile of the membrane potential $V(x, t)$ as a function of distance (in space constants) from the initial segment and time (in time constants). (d) Same as (c) as a function of time at different locations $x = 1.5$ (solid), 1 (dash-dot), 0.5 (dash) and 0 (dot). Parameters: $\bar{g} = 2$, $T_{up} = 0.1$, $T_r = 0.33$, $S = 10$, $x_1 = 1$, $x_2 = 1.5$, $L = 7$, $E = 60$, $E_{up} = 100$ and $E_{down} = -15$.

at the initial segment $V_A(t)$ exceeds the firing threshold S , the switch closes the first branch while the second branch is open and $V_A(t)$ is brought to V_{up} during a short period T_{up} . This simulates the rising phase of the action potential. Then the switch opens the first branch and closes the second branch so that $V_A(t)$ is brought to E_{down} , which simulates the descending phase of the action potential. The switch is opened after a period corresponding to the refractory period T_r (measured from the time of closing of the first branch, so $T_r > T_{up}$). If the switch was not reopened, T_r would be infinite and after time T_{up} the potential at x_2 would be clamped at E_{down} ; the receptor potential along the neuron in this case is given by (14) and shown in Fig. 3 for $E_{down} = 0$.

Model without passive backpropagation of action potentials. In Lánský *et al.* (1994) and Rospars *et al.* (1995) the action potentials were not assumed to propagate passively backward into the dendrite. The potential $V_A(t)$ of the initial segment was assumed to depend on the steady-state potential $V(x_2)$ at the initial segment x_2 , whereas $V(x_2)$ was assumed to be independent of the variations in time of $V_A(t)$. Thus the initial segment was not considered as a circuit incorporated in the cable, but merely as an independent circuit (Fig. 5a) driven by the dendritic current $I = V(x_2)/R_m$, where R_m is the membrane resistance of the lumped initial segment. We assumed also that the time constant $R_m C_m$ of the initial segment is equal to that of the dendrite cable $r_m c_m$.

This rough simplification permitted us to determine analytically the firing frequency f_a as a function of $V(x_2)$. Starting from the resting potential, for example, the potential $V_A(t)$ tends to rise exponentially to $V(x_2)$. If $V_A(t)$ exceeds the firing threshold S , an action potential is triggered as explained above. The firing frequency f_a is given by (see e.g. Tuckwell, 1988a; Rospars *et al.*, 1995)

$$f_a = \left\{ \ln \left(\frac{V(x_2) - E_{down}}{V(x_2) - S} \right) + T_r \right\}^{-1}, \quad V(x_2) > S. \quad (17)$$

Using the value of $V(x_2)$ from (13) in equation (17), we obtain an analytical solution for the firing frequency f_a as a function of the conductance \bar{g} .

Model with passive backpropagation of action potentials. The preceding model is not realistic because it does not take into account the backward effect of the action potential generating mechanism on the receptor potential. The generation of an action potential first charges and then discharges the cable, so that the receptor potential becomes a function of time $V(x, t)$, even in the case of a steady-state stimulation. This effect can be described

as a passive backpropagation of the action potential along the dendrite. In order to study backpropagation, the circuit representing the initial segment must be an integral part of the cable that describes the whole neuron (Fig. 5b) which gives a more satisfactory model of the neuron.

In this more realistic model no analytical solution of (1) is known for the chosen input signal (4). For this reason we have determined the receptor potential numerically. An example of the profile of the membrane potential $V(x, t)$ along the dendrite up to the initial segment x_2 is shown in Fig. 5c and d. These figures show that the peaks of the action potentials propagate to the distal end of the sensory dendrite, whereas their amplitude decreases and their shape becomes more rounded. The diminution of amplitude is faster when the conductance \bar{g} increases (not shown). The corresponding firing frequency is denoted f_b .

Comparison of model results with and without passive backpropagation of action potentials. As shown in Fig. 6a, in both models the firing frequency increases with the conductance \bar{g} . The maximum firing frequency f_{Mb} with backpropagation was approximately twice as large as that f_{Ma} without backpropagation for the set of parameters chosen. However, the curves of the relative firing frequencies f_a/f_{Ma} and f_b/f_{Mb} as a function of \bar{g} were very similar (Fig. 6b). It is desirable to see if this similarity holds also for other sets of parameters.

The firing frequencies f_a and f_b depends on six parameters: the threshold S , the duration T_{up} of the positive phase of the action potential, the total duration T_r of the action potential (refractory period), the battery

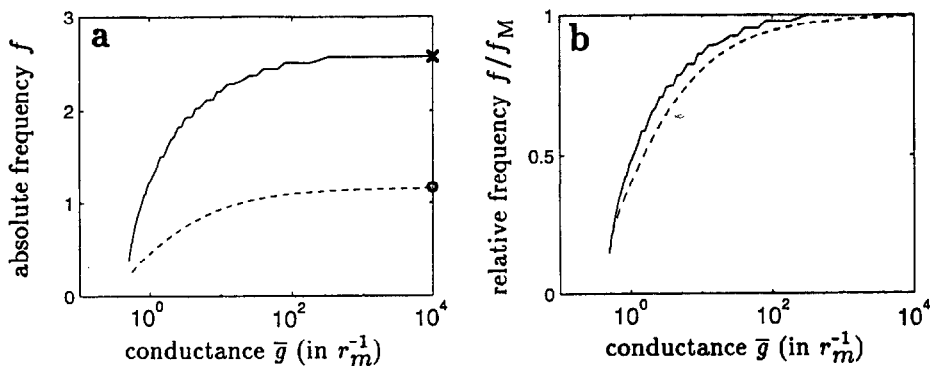


Figure 6. Firing frequency f in spikes per time constant (a) and relative firing frequency f/f_M (b) as a function of the conductance \bar{g} with (solid line) and without (dashed line) backpropagation of action potentials into the dendrite. In (a) the maximum firing frequency f_M with (cross, f_{Mb}) and without (circle, f_{Ma}) backpropagation are shown. Parameters are the same as in Fig. 5.

potentials E_{down} and E_{up} and the position of the initial segment with respect to the end of the sensitive dendrite (length of the passive dendrite $l_2 = x_2 - x_1$). Consider first how the ratio of the maximum firing frequencies f_{Mb}/f_{Ma} depends on these parameters (Fig. 7). This ratio was always greater than 1, which means that whatever the values of the parameters, the maximum firing frequencies for the model with backpropagation of action potentials is always greater than that without backpropagation. With all other parameters kept constant, f_{Mb}/f_{Ma} was found to be almost independent of T_{up} , E_{up} and l_2 (Fig. 7a, c, and e) for which only a slight linear increase is observed. The ratio was also observed to depend linearly on the threshold S (Fig. 7b) and the potential E_{down} (Fig. 7f), but with slightly greater slopes (upward for S ; downward for E_{down}). However, f_{Mb}/f_{Ma} was found to depend mostly on T_r (Fig. 7d); it decreases from about 6 for the smallest value of T_r ($T_r = T_{\text{up}} = 1/9$ membrane time constant, not shown) to about 2 for $T_r = 0.4$.

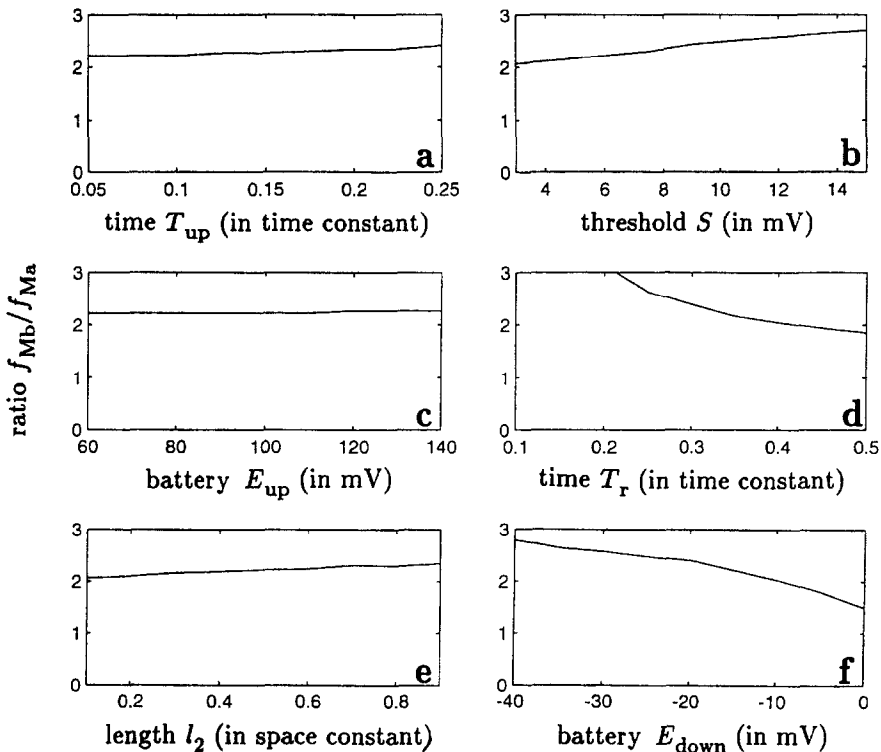


Figure 7. Ratio f_{Mb}/f_{Ma} of the maximum firing frequencies with and without backpropagation, as a function of time T_{up} (a), threshold S (b), battery E_{up} (c), time T_r (d), length $l_2 = x_2 - x_1$ (e) and battery E_{down} (f). Parameters are the same as in Fig. 5.

Compare now the relative firing frequencies f_a/f_{Ma} and f_b/f_{Mb} at four different values of the stimulation-dependent conductance $\bar{g} = 0.5, 1, 10$ and 10^4 when the parameters are varied one at a time (Fig. 8). For the largest value of \bar{g} (10^4) both firing frequencies are maximal whatever the parameter studied, so that $f_a/f_{Ma} = f_b/f_{Mb} = 1$. For any of the other values of \bar{g} , the relative firing frequencies with and without backpropagation depend in a similar way on the values of S , l_2 and E_{up} (Fig. 8a, c, and e) and display similar decrease when S and l_2 increase and E_{up} decreases. The ratios f_a/f_{Ma} and f_b/f_{Mb} are almost independent of T_{up} , T_r and E_{down} (Fig. 8b, d and f) over a large part of their studied ranges of variation, except in the case of the model with backpropagation for which the ratio f_b/f_{Mb} tends to 1 for small values of T_r and E_{down} and large values of T_{up} .

In conclusion, with the studied values of the parameters, the relative firing frequency without backpropagation f_a/f_{Ma} can be considered as a good approximation of the relative firing frequency with backpropagation

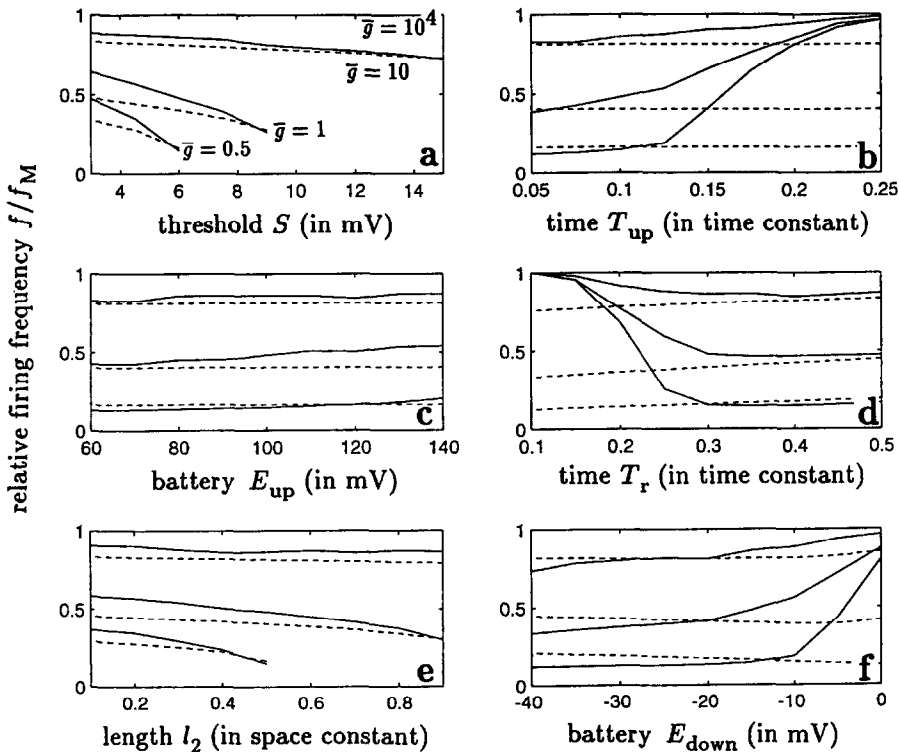


Figure 8. Relative firing frequency f_a/f_{Ma} without (dashed lines) and f_b/f_{Mb} (solid lines) without backpropagation as a function of conductance \bar{g} ($= 10^4, 10, 1$ and 0.5) and threshold S (a), time T_{up} (b), battery E_{up} (c), time T_r (d), length $l_2 = x_2 - x_1$ (e) and battery E_{down} (f). Parameters are the same as in Fig. 5.

f_b/f_{Mb} except for some values of T_{up} , T_r and E_{down} . For these values the curve of f_b as a function of \bar{g} is such that the neuron either does not respond at all (for \bar{g} below a certain threshold) or responds with maximal firing frequency (above this threshold), so that the coding range is very narrow.

5. Discussion. The olfactory receptor neuron is described as a cylindrical cable of constant diameter and finite length L divided into three parts; a sensory segment, a passive segment and an axon (Fig. 1a). The sensory dendrite is assumed to possess a uniform density of receptor sites and ion channels and to be uniformly stimulated by odorant molecules at constant concentration. The transduction mechanisms involved in the concentration-to-conductance conversion are not considered in the present article (see Lamb and Pugh, 1992; for a simplified transduction model, see Kaissling, 1971 and Rospars *et al.* 1995), which focuses on the conductance-to-voltage and voltage-to-frequency conversion steps. The properties of these conversion steps, which takes place at the dendrite and axon initial segments, respectively, depend on the neuron length and the passive invasion of the dendrite by the action potentials.

Effect of neuron length on the receptor potential. In the neuron model considered, the receptor potential along the neuron arises from a uniform conductance change at the sensory dendrite. Its spatial spreading is given by (13) and shown in Fig. 2. This solution is a generalization for any neuron length of the equations given in Rospars *et al.* (1995) for a semi-infinite cable.

The coding performance of the receptor potential depends on the properties of the conductance-to-voltage conversion function, that is, on the receptor potential at the initial segment as a function of the conductance change \bar{g} at the sensory dendrite (Fig. 4a). The graph of this function is of sigmoid shape and can be characterized by its coding range and its position along the conductance axis. The inclusion of the spatial extent of the receptor neuron has a significant effect on both features. This conclusion is of interest because the point model neuron is commonly used (Segev, 1992).

The position of the curve can be characterized by the value of \bar{g} for which the receptor potential is 50% of its maximum value. This conductance is the smallest for a neuron in which there is no odorant-insensitive part, i.e. $L - x_1 = 0$ (equivalent to a point model neuron). Consequently, a short neuron can respond at lower odorant concentrations than a long one.

The coding range can be quantified by the distance between the values of \bar{g} for which the potential increases from e.g. 5 to 95% of its maximum value. The shortest coding range is obtained in a point model neuron for

which the coding range is about 2.5 decades, i.e. the receptor potential goes from 5 to 95% of its maximal value when the conductance is multiplied by $10^{2.5} = 316$. The largest coding range (close to 3.5 decades, i.e. 3160) is obtained for a semi-infinite neuron, which is the case in practice for a neuron whose length is four space constants or more (Fig. 4b). Moreover, the neuron length L does not change greatly the threshold conductance, but mostly the saturating conductance (Fig. 4c). This means that lengthening the neuron extends the coding range at high odorant concentrations. Thus, a long neuron gains in coding range and sensitivity at high concentrations but at the expense of losing sensitivity at low concentrations.

Effect of dendritic passive backpropagation of action potentials. During its passive backpropagation into the dendrite, the amplitude of the action potential decreases rapidly and its shape becomes rounded. These effects can be interpreted as a consequence of the frequency-dependent voltage attenuation described by Spruston *et al.* (1994), who showed that in a cable, high-frequency voltage changes are much more attenuated than low-frequency voltage changes.

The passive backpropagation of action potentials into the dendrite increases (by a factor of about 2–3) the firing frequency with respect to the model without backpropagation. The direction of this effect might not be surprising in the cases where the backpropagation tends to raise the average value of the receptor potential, which in turn raises the firing frequency. However, the observed difference results mainly from the different circuits describing the axon in both models; in the model without backpropagation the initial segment is described by a lumped RC circuit unphysically attached to the dendritic cable in such a way that backpropagation cannot occur, whereas in the model with backpropagation, the circuit is imbedded in the cable and has complete continuity with the dendritic cable. This qualitative difference precludes a direct comparison of the firing frequencies in both models. This is the reason why we have used the relative firing frequency, i.e. the ratio of the frequency for a given odorant-sensitive conductance to the maximum frequency, which is obtained for a large conductance.

For most sets of parameters, the relative firing frequency was not changed significantly in the model without backpropagation. This indicates that the relative firing frequency for a given odorant-sensitive conductance can be approximated by that given by the analytical solution (13) (without backpropagation), except when the duration of the spike of the action potential is long, the refractory period is short and the posthyperpolarisation E_{down} is too close to the resting potential. So, conclusions based on the

analytical relative frequencies remain valid when backpropagation is taken in account.

These results encourage us to pursue the use of a Hodgkin–Huxley or Fitzhugh–Nagumo model of action potential generation instead of the phenomenological but useful approximation used here. Other extensions worth considering include the influence on the conductance range and the firing frequency of more complex neural geometries, such as branching dendrites and different diameters for the various components of the neuron (dendrite, soma, axon).

This research was supported by grant 309/95/0627 from the Grant Agency of the Czech Republic and a fellowship from Institut National de la Recherche Agronomique (to P.L.).

REFERENCES

- Abbott, L. F. 1992. Simple diagrammatic rules for solving dendritic cable problems. *Phys. A* **185**, 343.
- Abbott, L. F. 1994. Single neuron dynamics: An introduction. In *Neural Modeling and Neural Networks*, F. Ventriglia (Ed.). Oxford, UK: Pergamon Press.
- Butz, E. G. and J. D. Cowan. 1974. Transient potentials in dendritic systems of arbitrary geometry. *Biophys. J.* **14**, 661.
- Claiborne, B. J., A. M. Zador, Z. F. Mainen and T. H. Brown. 1992. Computational models of hippocampal neurons. In *Single Neuron Computation*, T. McKenna, J. Davis and S. F. Zornetzer (Eds.), p. 61. Boston, MA: Academic Press.
- Hodgkin, A. L. and W. A. H. Rushton. 1946. The electrical constants of a crustacean nerve fibre. *Proc. Roy. Soc. London Ser. B* **133**, 444.
- Kaissling, K.-E. 1971. Insect olfaction. In *Handbook of Sensory Physiology, IV: Chemical Senses*, L. M. Beidler (Ed.), Part 1. Berlin, Germany: Springer-Verlag.
- Kaissling, K.-E. 1986. Chemo-electrical transduction in insect olfactory receptors. *Ann. Rev. Neurosci.* **9**, 121.
- Kaissling, K.-E. 1987. *R. H. Wright Lectures on Insect Olfaction*, K. Colbow (Ed.). Burnaby, Canada: Simon Fraser University.
- Keil, T. A. 1984. Reconstruction and morphometry of silkmoth olfactory hairs: A comparative study of sensilla trichodea on the antennae of male *Antheraea polyphemus* and *Antheraea pernyi* (Insecta, Lepidoptera). *Zoomorphology* **104**, 147.
- Lamb, T. D. and E. N. Pugh Jr. 1992. G-protein cascades: gain and kinetics. *Trends in Neurosci.* **15**, 291.
- Lánský, P., J.-P. Rospars and A. Vermeulen. 1994. Basic mechanisms of coding stimulus intensity in the olfactory sensory neuron. *Neural Process. Lett.* **1**, 9.
- Mascagni, M. V. 1989. Numerical methods for neuronal modeling. In *Methods in Neural Modeling: From synapses to networks*, C. Koch and I. Segev (Eds.), p. 439. Cambridge, MA: The MIT Press.
- Rall, W. 1960. Membrane potential transients and membrane time constants of motoneurons. *Exp. Neurol.* **2**, 503.
- Rall, W. 1962. Theory of physiological properties of dendrites. *Ann. N.Y. Acad. Sci.* **96**, 1071.
- Rall, W. 1964. Theoretical significance of dendritic trees for neuronal input–output relations. In *Neural Theory and Modeling*, R. Reiss (Ed.). Stanford, CA: Stanford University Press.

- Rall, W. 1977. Core conductor theory and cable properties of neurons. In *Handbook of Physiology: The Nervous System*, E. R. Kandel (Ed.), Vol. 1. Bethesda, MD: American Physiological Society.
- Rall, W. 1989. Cable theory for dendritic neurons. In *Methods in Neural Modeling: From synapses to networks*, C. Koch and I. Segev (Eds.), p. 9. Cambridge, MA: The MIT Press.
- Rospars, J.-P., P. Lánský, H. C. Tuckwell and A. Vermeulen. 1995. Coding of odor intensity in a deterministic model of first-order olfactory neurons. *J. Comp. Neurosci.* To appear.
- Segev, I. 1992. Single neurone models: oversimple, complex and reduced. *Trends Neurosci.* **15**, 414.
- Segev, I., M. Rapp, Y. Manor and Y. Yarom. 1992. Analog and digital processing in single nerve cells: dendritic integration and axonal propagation. In *Single Neuron Computation*, T. McKenna, J. Davis and S. F. Zornetzer (Eds.), p. 173. Boston, MA: Academic Press.
- Spruston, N., D. B. Jaffe and D. Johnston, 1994. Dendritic attenuation of synaptic potentials and currents: role of passive membrane properties. *Trends Neurosci.* **17**, 161.
- Stengl, M., H. Hatt and H. Breer. 1992. Peripheral processes in insect olfaction. *Annu. Rev. Physiol.* **54**, 665.
- Tuckwell, H. C. 1988a. *Introduction to Theoretical Neurobiology*, Vol. 1. Cambridge, UK: Cambridge University Press.
- Tuckwell, H. C. 1988b. *Introduction to Theoretical Neurobiology*, Vol. 2. Cambridge, UK: Cambridge University Press.
- Vermeulen, A., J.-P. Rospars, P. Lánský and H. C. Tuckwell. 1995. Some new results on the coding of pheromone intensity in an olfactory sensory neuron. In *Third European Symposium on Artificial Neural Networks*, M. Verleysen (Ed.), p. 105. Brussels, Belgium: D. Facto.
- Wilson, C. J. 1992. Dendritic morphology, inward rectification, and the functional properties of neostriatal neurons. In *Single Neuron Computation*, T. McKenna, J. Davis and S. F. Zornetzer (Eds.), p. 141. Boston, MA: Academic Press.
- Walsh, J. B. and H. C. Tuckwell. 1985. Determination of the electrical potential over dendritic trees by mapping onto a nerve cylinder. *J. Theor. Neurobiol.* **4**, 2.

Received 25 June 1995